The signatures of large-scale patterns of atmospheric variability in Antarctic surface temperatures

Gareth J. Marshall[1] and David W. J. Thompson[2]

[1]British Antarctic Survey, Cambridge, UK, [2]Department of Atmospheric Science, Colorado State University, Fort Collins, Colorado, USA

Abstract We investigate the impact that the four principal large-scale patterns of Southern Hemisphere (SH) atmospheric circulation variability have on Antarctic surface air temperature (SAT): (1) the southern baroclinic annular mode (BAM), which is associated with variations in extratropical storm amplitude; (2) the Southern Annular Mode (SAM), associated with latitudinal shifts in the midlatitude jet; and (3) the two Pacific-South American patterns (PSA1 and PSA2), which are characterized by wave trains originating in the tropical Pacific that extend across the SH extratropics. A key aspect is the use of 35 years of daily observations and reanalysis data, which affords a sufficiently large sample size to assess the signatures of the circulation patterns in both the mean and variability of daily mean SAT anomalies. The BAM exerts the weakest influence on Antarctic SAT, albeit it is still important over select regions. Consistent with previous studies, the SAM is shown to influence SAT across most of the continent throughout the year. The PSA1 also affects SAT across almost all of Antarctica. Regionally, both PSA patterns can exert a greater impact on SAT than the SAM but also have a significantly weaker influence during summer, reflecting the seasonality of the SH response to El Niño–Southern Oscillation. The SAM and PSA patterns have distinct signatures in daily SAT variance that are physically consistent with their signatures in extratropical dynamic variability. The broad-scale climate linkages identified here provide benchmarks for interpreting the Antarctic climate response to future changes in tropical sea surface temperatures, ozone recovery, and greenhouse gas increases.

1. Introduction

Large-scale climate variability in the extratropical Southern Hemisphere (SH) atmospheric circulation is dominated by four principal patterns of atmospheric circulation variability: two so-called annular modes and two Pacific-South American (PSA) teleconnection patterns.

The SH annular modes consist of the well-known "barotropic" annular mode (usually referred to as the Southern Annular Mode or SAM) and its baroclinic counterpart (termed the baroclinic southern annular mode or BAM). Both patterns exhibit a high degree of zonal coherence or annularity [*Thompson and Wallace*, 2000]. The BAM emerges as the leading empirical orthogonal function (EOF) of extratropical eddy kinetic energy [*Thompson and Woodworth*, 2014]. It is linked primarily not to variations in the zonal mean flow but to variations in the amplitude of extratropical eddy activity over much of the Southern Hemisphere storm track. The SAM is the leading EOF of extratropical geopotential height and zonal mean kinetic energy [*Kidson*, 1988; *Hartmann and Lo*, 1998; *Thompson and Wallace*, 2000]. It has a robust barotropic component and is broadly characterized by north-south vacillations in the midlatitude zonal flow and the Southern Hemisphere storm track. Thus, the SAM is also frequently characterized as synchronous pressure anomalies of opposite sign above Antarctica and the midlatitudes [e.g., *Gong and Wang*, 1999; *Marshall*, 2003].

The PSA patterns are dominated by zonally asymmetric anomalies in the extratropical circulation, and are the SH analogue to the Pacific North-America pattern (the PNA) in the Northern Hemisphere (NH). Like the PNA, the PSA patterns are associated with out-of-phase geopotential height anomalies that stretch eastward across the extratropical Pacific Ocean from the tropical Pacific [e.g., *Kidson*, 1988; *Mo and Higgins*, 1998]. However, unlike the PNA, the PSA is not readily described by a single pattern but rather is associated with two structures, which together describe much of the variance in geopotential height in the SH extratropical Pacific sector. The so-called PSA1 and PSA2 patterns are frequently defined as the second and third EOFs of the extratropical geopotential height field [*Mo and Higgins*, 1998] (the first EOF corresponds to the SAM). The PSA patterns have their largest amplitude in the geopotential height field over the South Pacific sector of the

Southern Ocean, but they project onto the atmospheric circulation throughout much of the SH middle-high latitudes [e.g., *Kidson*, 1988; *Mo and Higgins*, 1998; *Raphael*, 2004; *Turner*, 2004].

The SAM and PSA patterns have been linked to various physical processes that contribute to their variability on interannual and secular timescales. The PSA 1 and PSA 2 patterns are correlated with variations in convection in the western and central tropical Pacific, respectively [*Mo and Higgins*, 1998], and thus, the PSA1 pattern closely resembles the broad-scale SH response to ENSO variability [e.g., *Mo and Higgins*, 1998; *Mo and Paegle*, 2001; *Schneider et al.*, 2012], particularly during austral spring [*Mo*, 2000; *Robertson and Mechoso*, 2003]. The PSA2 pattern has been linked to variations in central Pacific sea surface temperatures (SSTs) [e.g., *Rodrigues et al.*, 2015]. The SAM is associated with variations in the ENSO cycle during austral summer [*L'Heureux and Thompson*, 2006; *Fogt et al.*, 2011; *Schneider et al.*, 2012]. It has also exhibited a trend toward falling pressure over the polar cap during austral summer that is linked to the development of the Antarctic ozone hole [*Thompson and Solomon*, 2002; *Previdi and Polvani*, 2014]. The SAM is predicted to exhibit similar behavior in the future due to increasing greenhouse gases although ozone recovery is likely to at least partially negate this effect in austral summer [*Arblaster et al.*, 2011; *McLandress et al.*, 2011; *Polvani et al.*, 2011; *Sigmond et al.*, 2011]. The BAM exhibits variability on ~20–30 day timescales and thus may impart quasiperiodicity to meteorological fields averaged over large spatial scales [*Thompson and Barnes*, 2014].

Both the SAM and PSA patterns have also been linked to variations in Antarctic surface climate. The positive polarity of the SAM is associated with anomalously warm conditions across the Antarctic Peninsula and generally cool conditions across East Antarctica and much of West Antarctica [e.g., *Thompson and Solomon*, 2002; *Kwok and Comiso*, 2002; *Marshall*, 2007]. The cooler surface air temperatures (SATs) over East Antarctica are consistent with reduced poleward advection of heat and moisture [*Previdi et al.*, 2013] and a weakening of the strength of katabatic winds over the continent [*van den Broeke and van Lipzig*, 2003; *Marshall et al.*, 2013]. Conversely, the warmer SATs over the Peninsula are consistent with anomalous onshore flow of warm maritime air into the Peninsula region associated with a deeper Amundsen Sea Low [*Fogt et al.*, 2012b; *Hosking et al.*, 2013; *Raphael et al.*, 2016], which forms a marked nonannular component to the SAM west of the Peninsula [e.g., *Fogt et al.*, 2012a]. The PSA1 pattern is connected to variations in SATs over the Peninsula and parts of West Antarctica [*Schneider et al.*, 2012]. The recent winter warming in West Antarctica has also been linked to increases in sea surface temperatures (SSTs) in the central tropical Pacific [*Lee et al.*, 2010; *Ding et al.*, 2011] and can therefore be linked to changes in the PSA 2 pattern. As far as we know, the impacts of the BAM on Antarctic climate have not been examined in previous work.

The goal of this paper is to build on previous work by providing a comprehensive analysis of the impact on Antarctic SATs associated with both annular modes and PSA patterns. A major innovation of the paper is its emphasis on daily mean data, which provides two key advantages: (1) it allows us to examine the climate impacts of internal atmospheric variability with a much larger sample size than that available from monthly or seasonal mean data (i.e., SAT and large-scale atmospheric variability exhibit variations on submonthly timescales) and (2) it allows us to assess the signatures of large-scale atmospheric variability in not only the mean but also the daily variance of Antarctic surface climate. We focus specifically on the four principal patterns of internal atmospheric variability in the extratropical SH. Hence, we do not explicitly consider the SH response to ENSO, which has been examined extensively in previous work [e.g., *Turner*, 2004; *Schneider et al.*, 2012; *Wilson et al.*, 2014]. However, as noted in the studies cited above, ENSO is implicit in analyses based on both the SAM and one of the PSA patterns, particularly during austral summer. Data are discussed in section 2 with an explanation of how an effective sample size is calculated given in the supporting information. Section 3 reviews the patterns of variability used in the analysis, and section 4 describes their signatures in Antarctic SATs. We limit the figures in the main text to an analysis of annual data, but because there are known seasonal differences in the impact of the patterns of variability, key seasonal differences are described in the text and seasonal figures are included in the supporting information. Discussion and concluding remarks are provided in section 5.

2. Data

The analyses draw from daily mean output from two data sources: (1) 18 Antarctic stations (17 staffed and 1 automatic weather station (AWS)) and (2) the European Centre for Medium Range Weather Forecasts (ECMWF) ERA-Interim reanalysis [*Dee et al.*, 2011]. Daily station values of SAT from the 35 year period of
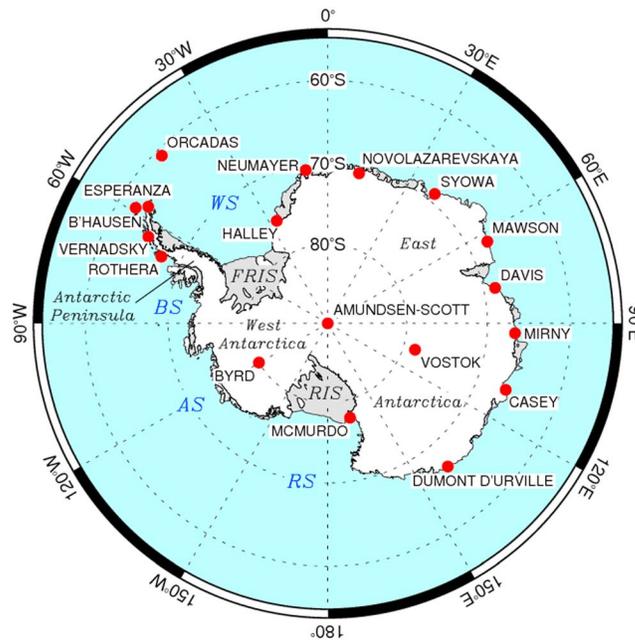
Figure 1. Location map of the 18 Antarctic meteorological stations used in this study and place names used in the text; AS is Amundsen Sea, BS is Bellingshausen Sea, FRIS is Filchner-Ronne Ice Shelf, RIS is Ross Ice Shelf, RS is Ross Sea, and WS is Weddell Sea.

1979–2013 are derived as the mean of the four synoptic (6-hourly) observations and only when all four are available. The station observations were derived primarily from the archive used to produce the Scientific Committee on Antarctic Research Reference Antarctic Data for Environmental Research monthly database [*Turner et al.*, 2004]. Byrd AWS is included because there are currently no long-term staffed stations operational in West Antarctica, and this site is known to be among the most rapidly warming regions on Earth [*Bromwich et al.*, 2013]. Station locations are shown in Figure 1, and data availability is given in Table 1. The latter varies from 71.6% at Byrd to almost 100% at Syowa, Dumont D'Urville, and Vernadsky, with a mean across the stations of 95.7%.

All daily SAT data are converted to anomalies by subtracting the long-term mean annual cycle for 1979–2013 from each station/grid point. Mean data for 29 February is calculated as a weighted mean of observations/data from 28 and 29 February and 1 March. The significance of the differences between two sample populations is derived using a two-tailed test of the t statistic. The significance of ratios in the standard deviations of daily SAT between the two phases of a circulation pattern (section 3) is assessed using the F statistic. Results are considered statistically significant if there is less than a 5% chance that they could arise by chance ($p < 0.05$). Autocorrelation is accounted for as per *Wilks* [2006] when calculating any statistics: this is especially important when using daily data. An explanation and justification for using this method is given in the supporting information. The effective sample size for the 18 stations across the 35 years varies from 1420 to 2322, whereas the original number of samples

Table 1. Comparison of Daily ERA-Interim SAT Values Against Observations for 1979–2013

Station	Data Availability	$\overline{\Delta T}$ (°C)	Δrmse (°C)	σ ratio	r
Amundsen-Scott	99.5%	4.53[a]	1.16	0.72[a]	0.97
Novolazarevskaya	99.4%	−3.20[a]	0.42	1.06[a]	0.97
Syowa	100.0%	0.29	1.32	0.84[a]	0.99
Mawson	99.6%	−4.82[a]	0.44	1.23[a]	0.97
Davis	99.6%	−0.12	1.46	0.88[a]	0.99
Mirny	99.2%	−0.91[a]	0.68	0.96[a]	0.98
Vostok	91.1%	4.63[a]	0.76	0.78[a]	0.98
Casey	99.8%	−1.00[a]	0.52	0.94[a]	0.99
Dumont D'Urville	100.0%	−3.94[a]	0.45	1.16[a]	0.98
McMurdo	84.7%	−4.82[a]	1.12	1.01	0.96
Byrd	71.6%	0.75	1.91	0.89[a]	0.97
Rothera	99.3%	−2.02[a]	0.76	0.98	0.95
Vernadsky	100.0%	−1.85[a]	0.88	1.01	0.92
Bellingshausen	99.8%	0.42[a]	0.65	0.98	0.97
Esperanza	94.2%	0.43	2.70	0.80[a]	0.90
Orcadas	92.2%	−0.09	1.12	0.92[a]	0.98
Halley	99.7%	2.35[a]	1.59	0.77[a]	0.97
Neumayer	93.5%	3.27[a]	1.32	0.68[a]	0.95

[a]When the mean or variance is significantly different at the $p < 0.05$ level.

ranged from 9148 to 12783 (Table S1). If the robustness of the results is in doubt, for example, if the regions of significance are small and isolated, they are further tested by splitting the time series into halves and repeating the analysis.

The ERA-Interim SAT data were obtained on a Gaussian N128 grid, which has a spatial resolution of ~80 km. Among several advances over the previous ECMWF reanalysis is an improved representation of the hydrological cycle. *Bracegirdle and Marshall* [2012] demonstrated that ERA-Interim is currently the best reanalysis for depicting Antarctic climate. Nevertheless, using monthly data, *Jones and Lister* [2015] found that some significant biases and differences in variability in Antarctic SAT do exist within ERA-Interim as compared to station observations, while *Nicolas and Bromwich* [2014] describe temporal fluctuations in Antarctic SATs not observed in other reanalyses. ERA-Interim data gridded at a regular 1.25° grid were utilized to derive the four patterns of atmospheric circulation variability (section 3). In addition, other ERA-Interim data were used at Gaussian N80 resolution (~125 km); these include the near-surface wind components and the 850 hPa meridional wind component and temperature.

Discrepancies between observed and reanalysis SAT data are summarized in Table 1. The comparisons in Table 1 are based on the 35 year period examined, and the reanalysis data interpolated to the station location to the nearest 0.1° latitude/longitude. The bias or differences in *total* (not anomalous) mean SAT (column labeled $\overline{\Delta T}$, defined as ERA-Interim minus observations) have little bearing on our results since we are interested in the variability in Antarctic temperature. Nevertheless, it is interesting to note that they range from 0.09°C at Orcadas to a substantial 4.82°C at Mawson and McMurdo. The differences in mean temperature arise in part from errors in the ERA-Interim topography over Antarctica [*Bracegirdle and Marshall*, 2012]. The next column (Δrmse) reflects the errors in the reanalysis around this "fixed" bias and is calculated as the root mean square error minus the magnitude of $\overline{\Delta T}$: values range from 0.42°C at Novolazarevskaya to 2.70°C at Esperanza, with a mean of 1.07°C.

The ratio of standard deviations in *anomalous* data (column labeled σ ratio, defined as ERA-Interim divided by observations) reveals that the reanalysis has lower variance in daily mean Antarctic SAT at 13 out of 18 station locations. Ratios range from 0.68 at Neumayer to 1.23 at Mawson, and the daily SAT variability is significantly different at 14 stations (cf. Table 1). However, the correlation coefficients between the *anomalous* station-based data and ERA-Interim are uniformly above 0.90. Thus, despite the differences in SAT variance between observations and ERA-Interim at several locations across Antarctica, we do not expect this will qualitatively influence the primary findings of the study. Reference will be made to Table 1 when results from the two data sets disagree.

3. Patterns of Atmospheric Variability

The patterns of variability examined here were calculated from EOF analysis of daily ERA-Interim output for 1979–2013. In all cases, the data are weighted by the square root of the cosine of latitude. For the BAM and SAM, they are also weighted by the mass represented by each vertical level.

The BAM is defined as the leading EOF of the anomalous daily mean, zonal mean eddy kinetic energy $[u^{*2} + v^{*2}]/2$ over all levels between 1000 and 200 hPa and latitudes 20–70°S, where u and v denote the zonal and meridional wind components, respectively, and square brackets denote the zonal mean and asterisks departures from the zonal mean. Daily mean values of the BAM index time series are defined as the corresponding principal component (PC) time series. Note that in practice, the BAM index time series is effectively identical to the simple hemispheric average of eddy kinetic energy (EKE) anomalies [*Thompson and Woodworth*, 2014]. The SAM, PSA1, and PSA2 are defined as the leading second and third EOFs of monthly mean 500 hPa geopotential height anomalies, respectively. Daily mean expansion coefficient time series of the SAM and PSA patterns are found by projecting daily mean 500 hPa geopotential height anomalies onto the resulting EOF patterns. The resulting BAM, SAM and PSA time series are standardized so that they have a mean of zero and a standard deviation of one.

The variances associated with the EOFs used in this study are listed in Table 2. The leading EOF of eddy kinetic energy used to define the BAM is well separated from higher order EOFs as per the *North et al.* [1982] criterion. The leading EOF of 500 hPa geopotential height used to define the SAM is well separated from the second EOF [e.g., *Kidson*, 1988; *Thompson and Wallace*, 2000]. However, the second and third EOFs of 500 hPa geopotential height used to define the PSA patterns are not well separated from each other

Table 2. Variance Explained by the EOFs Used in This Study Together With an Estimate of Their Uncertainty Using the *North et al.* [1982] Criterion[a]

Data Set	EOF1	EOF2	EOF3	EOF4
Daily mean and zonal mean EKE over 1000–200 hPa, 20–70°S	34 ± 2%(BAM)	19 ± 1%	11 ± 0%	7 ± 0%
Monthly mean Z500 20–90°S	42 ± 3%(SAM)	8 ± 1%(PSA 1)	7 ± 1%(PSA 2)	5 ± 0%

[a]Values are given to the nearest 1% as this is likely the accuracy of the estimates.

[*Kidson*, 1988; *Mo and Higgins*, 1998]. Nevertheless, similar PSA patterns also emerge as the second and third EOFs of geopotential height anomalies at other tropospheric levels [*Kidson*, 1988; *Mo and Higgins*, 1998] and from daily mean geopotential height (not shown). Taken together, the two PSA patterns used here are reproducible from a variety of analysis designs and periods.

Note that the patterns studied here are not significantly correlated with each other. The relationships between the BAM and SAM are not statistically significant at any lag [*Thompson and Woodworth*, 2014]. Furthermore, by construction, the SAM, PSA1, and PSA2 indices are linearly orthogonal on monthly timescales.

The structures of the annular modes and PSA patterns in the large-scale SH atmospheric flow and their signatures in the meridional eddy fluxes of heat are reviewed briefly in Figure 2. Note that over the
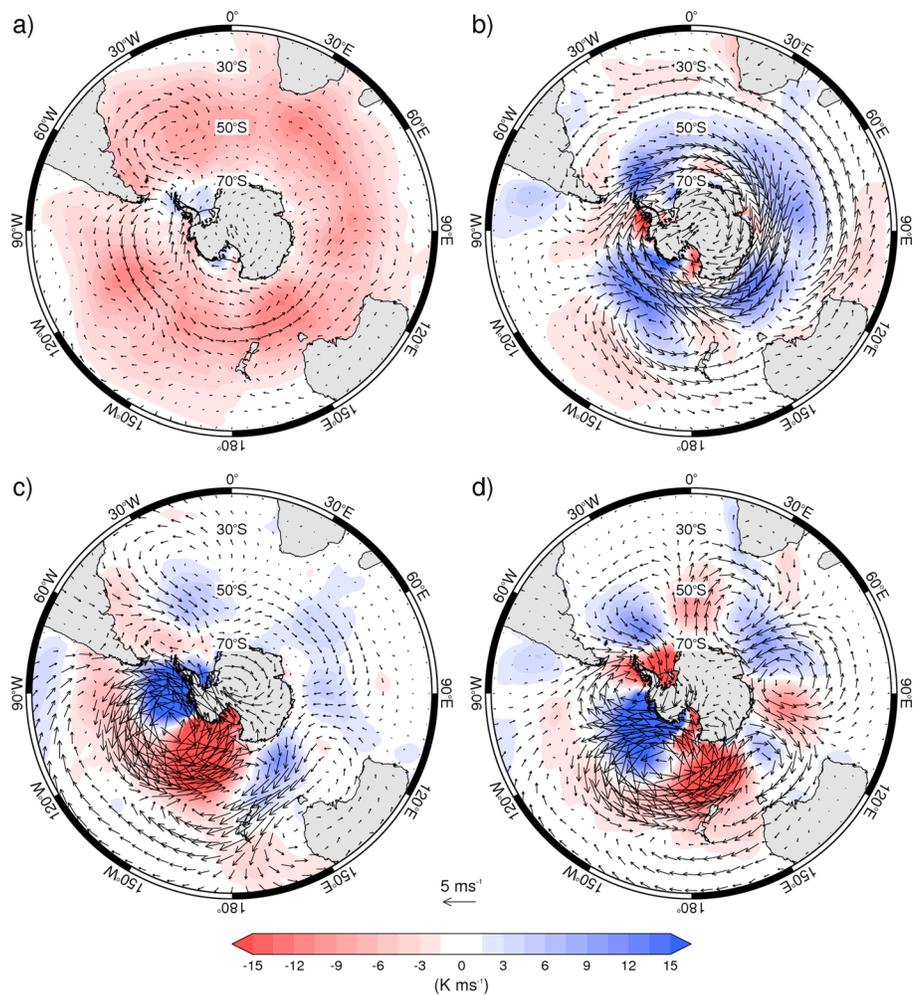
Figure 2. Differences in mean daily meridional heat flux anomalies ($v^{*}T^{*}$) at 850 hPa (shading) and near-surface winds (vectors) across all seasons between the positive and negative polarities of (a) the BAM, (b) the SAM, (c) the PSA1 pattern, and (d) the PSA2 pattern. Negative (red shading) values denote anomalously poleward heat fluxes.

Table 3. The Number of Days in Each Phase of the Atmospheric Circulation Patterns

Phase	Annual	Fall	Winter	Spring	Summer
BAM+	2020	555	510	447	508
BAM−	2046	553	491	483	519
SAM+	1997	451	638	515	393
SAM−	1998	411	665	547	355
PSA 1+	2002	514	617	550	321
PSA 1−	2097	551	636	574	336
PSA 2+	2107	510	708	518	371
PSA 2−	2039	535	673	489	342

Southern Ocean, the eddy flux of heat is largely dominated by synoptic scale eddies; anomalously poleward (that is, negative) eddy heat fluxes are consistent with enhanced synoptic eddy activity and vice versa. The results show composite differences in meridional eddy heat flux at 850 hPa ($v^{*}T^{*}850$) (shading) and near-surface winds (vectors) between positive and negative days in the respective indices. Positive and negative days are defined as those when the index values are greater than +1 and less than −1, respectively (i.e., ±1 standard deviation). The positive polarity of the BAM is defined when there are anomalously poleward (southward) eddy fluxes of heat; the positive polarity of the SAM is defined in the standard way (anomalously low pressure over Antarctica) and the polarity of the PSA patterns are defined according to Figures 4b and 4c of *Kidson* [1988]. The number of positive and negative days used in the composite analyses for each of the four circulation patterns is given in Table 3. Note that Figures 2, 3, and S1–S4 show differences as positive minus negative days for the patterns of circulation variability; thus, the sign of the difference is equivalent to the sign of anomalies associated with the positive polarity of these patterns.

The positive polarity of the BAM (Figure 2a) is marked by hemispheric-scale increases in the poleward eddy heat flux at SH midlatitudes between 30 and 60°S and centered at ~50°S but relatively little change in the eddy heat flux at Antarctic latitudes (note that the eddy heat fluxes would be somewhat larger if they were shown for the period ~1–3 days prior to peak amplitude in the BAM index; see Figure 4b of *Thompson and Woodworth* [2014]). Variations in the BAM are associated with only weak anomalies in the near-surface flow around the continent (Figure 2a). In contrast, the positive polarity of the SAM (Figure 2b) is linked to robust changes in the surface flow, with anomalously westerly circumpolar flow at ~60°S and easterly flow along ~40°S. The meridional eddy heat flux anomalies concomitant with the positive polarity of the SAM are generally equatorward over the Southern Ocean around Antarctica. The equatorward eddy heat flux anomalies associated with the SAM are very short lived (they persist only a few days), and integrated over a week or longer are much weaker than those associated with the BAM [*Thompson and Woodworth*, 2014, cf. Figure 4a]. However, we note that the positive polarity of the SAM is also linked with two regions of anomalous poleward heat fluxes south of the main storm track, in the Bellingshausen Sea west of the Peninsula and in the eastern Ross Sea (Figure 2b).

The positive polarity of the PSA1 pattern is dominated by anticyclonic wind anomalies in the South Pacific sector of the Southern Ocean (Figure 2c). As noted in section 1, the pressure anomalies associated with the PSA1 pattern also emerge in composites based on the ENSO cycle [e.g., *Mo and Higgins*, 1998; *Mo and Paegle*, 2001; *Schneider et al.*, 2012]. The anticyclonic center of action centered at ~120°W is linked to anomalously offshore flow and reduced eddy activity in the Peninsula region but anomalously onshore flow and increased eddy activity into the Ross Sea. The surface wind anomalies associated with the positive phase of the PSA 2 pattern (Figure 2d) are similar to those linked with PSA 1 but for two notable differences: (1) the primary anticyclonic center of action is located further west and is centered near ~150°W in the Ross Sea and (2) the anomalies are hemispheric-wide in the SH extratropics such that the PSA2 pattern has a more pronounced impact on atmospheric circulation than PSA1 over much of the southern Atlantic and Indian Ocean sectors. However, the most robust anomalies associated with the positive PSA2 pattern include anomalously onshore winds and poleward eddy heat fluxes into the western Ross Sea and eastern part of East Antarctica and anomalously offshore winds and equatorward heat fluxes emanating from near West Antarctica.

As summarized in Figure 2, the BAM, SAM, and two PSA patterns all have very different projections on the atmospheric circulation around Antarctica. In the following section, we explore the attendant differences in their impacts on SATs across the Antarctic continent.
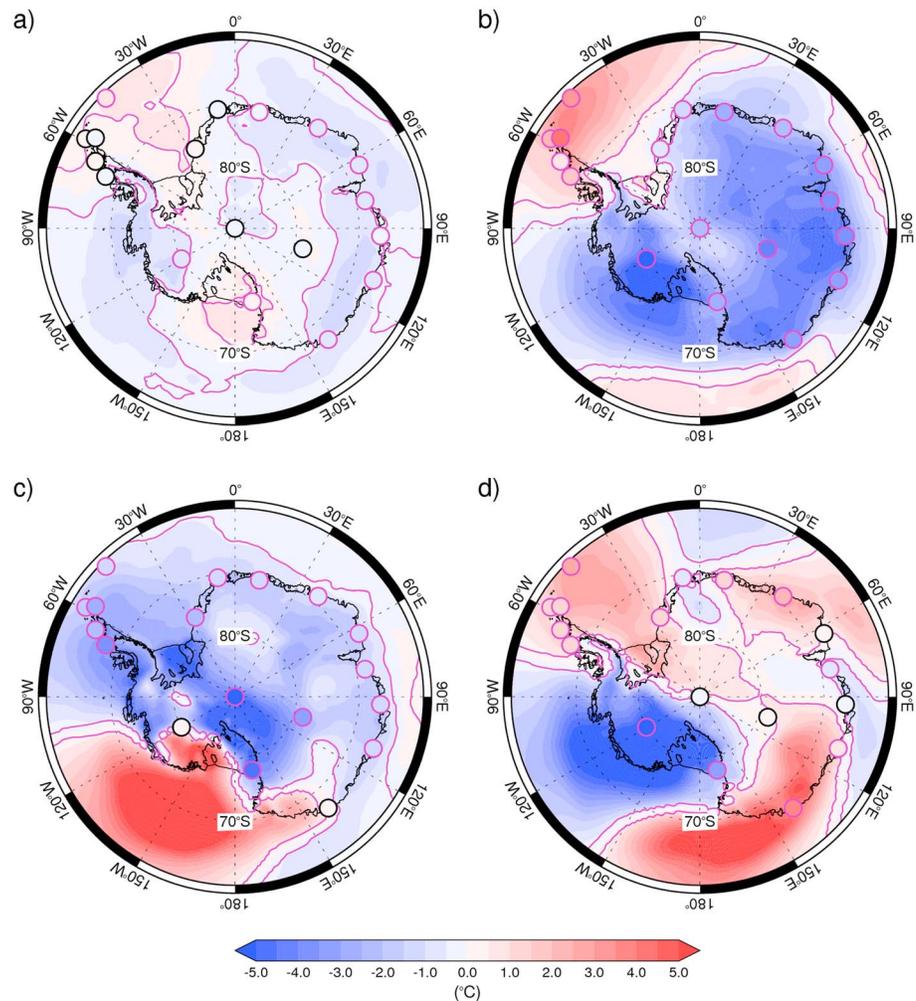
Figure 3. As Figure 2 but for the differences in mean daily SAT anomalies. The purple contour represents regions where the difference is significant at the $p < 0.05$ level. Similarly, stations where the difference is significant at the $p < 0.05$ level are represented as a purple circle.

4. The Impacts of Large-Scale Atmospheric Variability on Antarctic Surface Temperatures

4.1. Daily SAT Anomalies

Here we examine the differences in daily mean Antarctic SAT anomalies between positive and negative days of the annular modes and PSA patterns across all seasons (Figure 3). Individual seasons are shown in the supporting information (Figures S2–S5), and any significant seasonal differences are discussed in the text. We have checked our results using "pure" composite analyses that remove the potential influence of the other patterns; e.g., the "pure" BAM composite difference refers to that between positive and negative days of the BAM index calculated only for days when the amplitude of the SAM and both PSA patterns are all neutral. The results are, within sampling variability, generally indistinguishable from the overall results, with any exceptions noted in the text.

Composite differences in SAT anomalies between all positive BAM and negative BAM days are shown in Figure 3a. The results reveal modest but statistically significant negative temperature anomalies (defined using the $p < 0.05$ level) over the majority of Antarctica. In particular, the positive polarity of the BAM leads to cooling over much of coastal East Antarctica and inland up to ~3000 m in elevation, most of West Antarctica and the southern Peninsula. However, we note the widespread significance across the first of these regions disappears when using the "pure" BAM composite difference, suggesting it is not a robust response. The only two areas of significant warming over the continent according to ERA-Interim are (1) the very northern Antarctic Peninsula and the region to the north-

east that incorporates Orcadas station in the South Orkney Islands and (2) a small part of the Ross Ice Shelf that includes McMurdo station. Again, the differences in anomalies in both these regions are relatively weak and on the fringe of statistical significance. The SAT anomaly differences derived from ERA-Interim data are generally consistent with those derived from the station-based observations. In results based on all seasons (Figure 3a), the greatest observed negative difference in anomalies is found at Byrd (–0.8°C), while the greatest positive difference is found at Orcadas (0.6°C). Results stratified by season reveal that the relationship between the BAM and Antarctic SATs is much weaker during summer (Figure S2).

Analogous results for the SAM are shown in Figures 3b and S2. Overall, the SAM has a much greater impact on Antarctic SATs than the BAM. The pattern of anomalously warm SATs over the northern Peninsula and cool SATs across both West and East Antarctica during the positive polarity of the SAM has been widely established in previous work based on monthly mean data [*Thompson and Solomon*, 2002; *Kwok and Comiso*, 2002; *Marshall*, 2007]. Here we demonstrate that the structure of the SAM in Antarctic SAT is readily reproduced in daily SAT anomaly data from ERA-Interim, from the station-based observations, and in all four seasons (Figure S3). The only regions of Antarctica in which significant differences in SAT anomaly do not exist between the positive and negative polarities of the SAM are the southern part of the Peninsula and an area of the Filchner-Ronne Ice Shelf. The greatest negative differences in daily SAT anomalies between the two polarites of the SAM occur in the Marie Byrd Land region of West Antarctica that includes Byrd (where the station-based difference is a substantial –5.3°C) and in parts of East Antarctica (Figure 3b). In both ERA-Interim and the observations there is a positive SAT difference across most of the Peninsula, extending further south on the west coast. The largest SAT differences are found at Esperanza (located on the east side of the Peninsula, cf. Figure 1), where the station-based anomaly difference is 4.2°C. The increases in Esperanza SAT have been linked to the advection of warm air from west to east over the Peninsula and the related föhn effect on the lee side where the station is located [*Marshall et al.*, 2006]. In addition, *Marshall et al.* [2006] demonstrated that regression coefficients between SAT and the SAM are 3 times greater on the east side of the Peninsula than the west. Analysis of the seasonal data (Figure S3) suggests that the longitudinal differences in SAT anomalies across the Peninsula are robust across the year, as expected given the föhn effect is prevalent during all seasons [*Cape et al.*, 2015] but that the amplitude of the results varies between ERA-Interim and the station-based observations, particularly during summer.

The composite differences for Antarctic daily mean SAT anomalies between positive and negative PSA1 days are shown in Figure 3c. As expected from the pattern of wind anomalies in Figure 2c, the impact of the PSA1 pattern on Antarctic SAT is most pronounced over the South Pacific region. Nevertheless, as is the case for the SAM, the PSA1 pattern has a significant impact on SAT across almost the entire continent. The positive polarity of the PSA1 pattern is associated with warming over the eastern Ross Ice Shelf and adjacent parts of West Antarctica. But it is linked with cooling over almost the entirety of the rest of the continent, including those parts of East Antarctica on the opposite side of the continent to the South Pacific. The station observations indicate a very similar spatial pattern: all have significant negative SAT anomaly differences except for Byrd and Dumont D'Urville, which lie in a narrow band between regions with significant positive and negative differences in SAT anomalies (Figure 2c). The largest observed differences are found at Amundsen-Scott (–5.5°C). Results stratified by season (Figure S4) indicate that the pattern found in year-round data is evident in all seasons but is much weaker in summer (Figure S4d). Nevertheless, significant differences in SAT anomalies are observed at the majority of Antarctic stations, including Davis, where summer SATs have been shown to be influenced by ENSO [*Schneider et al.*, 2012].

Figure 3d shows equivalent results for the PSA2 pattern. As is the case for the circulation anomalies (Figure 2d), the SAT anomalies over Antarctica include a wave 3 component in both ERA-Interim and station observations. Unsurprisingly, the largest differences are found on opposing sides of the high pressure anomaly in the South Pacific. The greatest warming in positive relative to negative PSA2 is 3.5°C is at Dumont D'Urville, located in coastal East Antarctica, where the anomalous flow is onshore (Figure 2d), while the greatest cooling is –7.2°C at Byrd, in West Antarctica, associated with anomalous offshore flow (Figure 2d) (the latter is the largest observed daily SAT anomaly difference in this study). Significant SAT anomalies are also found in regions of anomalously northwesterly flow over the northern Peninsula (compare Figures 2d and 3d) and over much of coastal East Antarctica. Regions where there is no significant signal of the PSA2 pattern in Antarctic SAT are found over the Plateau, including at Amundsen-Scott and Vostok, and the southern half of the Peninsula. As is the case for the PSA1 pattern, the seasonally stratified results (Figure S5) demonstrate that the linkages
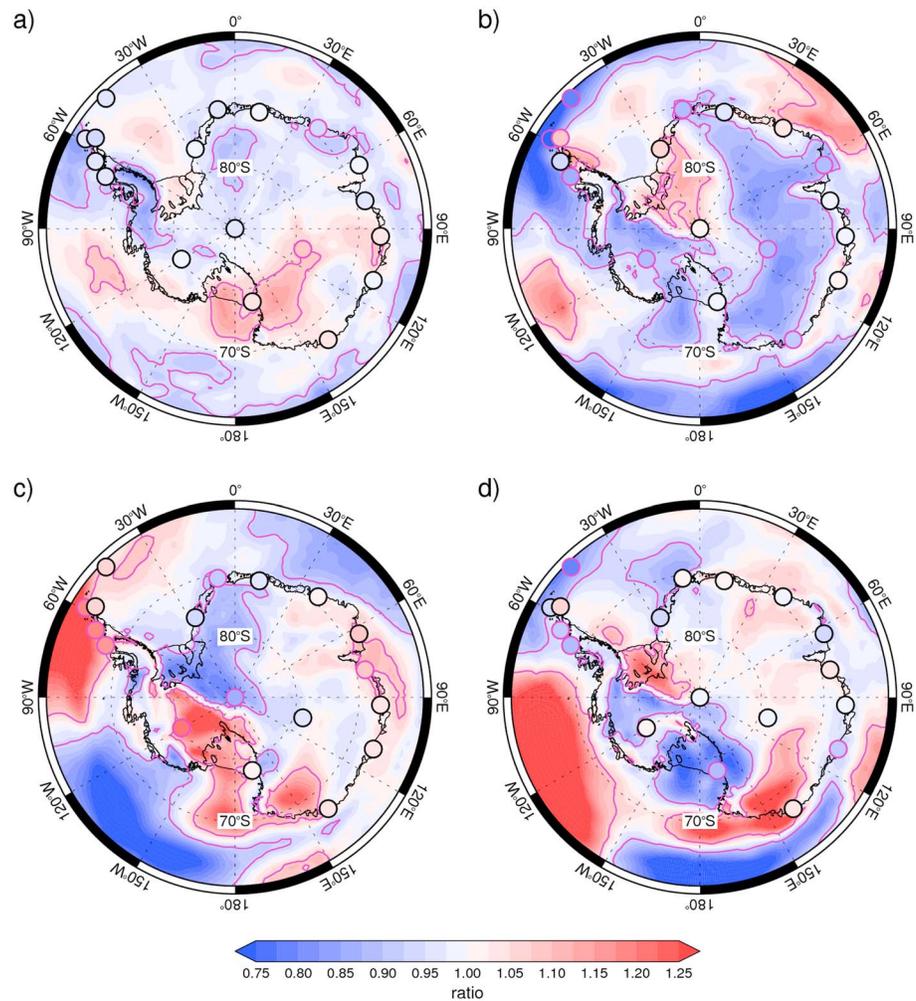
Figure 4. As Figure 3 but for the ratio of daily SAT anomaly standard deviation. The purple contour represents regions where the ratio is significantly different from unity at the $p < 0.05$ level. Similarly, stations where the ratio is significantly different from unity at the $p < 0.05$ level are represented as a purple circle.

between the PSA2 pattern and Antarctic SAT are weakest during summer. Interestingly, the pattern of SAT anomalies associated with the PSA2 pattern—particularly the out-of-phase relationship between SATs over the Peninsula and West Antarctica—is similar to that shown by *Ding et al.* [2011], who examined the impact of central Pacific SSTs on Antarctic winter SATs (their Figure 3). The results shown here suggest that the PSA 2 has a similar impact on SATs in fall and spring.

It is worth emphasizing that the impacts of the PSA patterns on Antarctic SATs have their weakest amplitude during summer, whereas the impacts of the SAM have a comparable amplitude during all seasons. The seasonality of the Antarctic impacts of the PSA patterns is consistent with the seasonality of the SH response to ENSO, which peaks during austral spring but weakens rapidly during summer [*Jin and Kirtman*, 2009; *Schneider et al.*, 2012].

4.2. Daily SAT Variability

In this section, we undertake a similar analysis but investigate the signatures of the SAM, BAM, and PSA patterns in the standard deviation (rather than the mean) of daily mean SAT anomalies. For all patterns, we show the ratio of the standard deviations (hereinafter written as σ ratio) between the composite samples for the positive and negative polarities (thus, if the σ ratio is greater than 1, SAT variability is greater in the positive polarity of the circulation index and vice versa). The significance is tested using the *F* statistic and, in select cases, the robustness of key features is assessed by examining results in the first and second halves of the

data record. Similar to the previous section, Figure 4 shows results for all calendar days; results stratified by season are provided in the supporting information Figures S6–S9.

The positive polarity of the BAM is associated with notable increases in the variance of daily mean lower tropospheric temperatures at *middle* latitudes, consistent with its signature in eddy amplitudes [*Thompson and Woodworth*, 2014, cf. Figure 10d]. However, as evidenced in Figure 4a, it has only a modest signature in SAT variance over Antarctica. Regions of significant decreases in Antarctic SAT variance during the positive polarity of the BAM are found over the southern and northern tip regions of the Antarctic Peninsula and small areas of East Antarctica (Figure 4a). Regions of significant increases are found over parts of eastern East Antarctica and the Ross Ice Shelf, extending inland as far as Vostok on the Plateau. The Peninsula and Ross Ice Shelf/Plateau features are reproducible in subsets of the data for the first and second halves of the record (not shown). However, the other regions of apparent significance, which are generally small and scattered, are not. The ratios at the stations are only statistically significantly different from unity at Syowa and Vostok. Furthermore, the patterns of variance ratios are not consistent across all seasons, and in some regions the BAM can have opposing impacts on the magnitude of SAT variability from one season to the next (Figure S6). For these reasons, we view the signature of the BAM in Antarctic SAT variability as weak and of relatively little climatic interest.

The SAM has a much more robust signature in Antarctic SAT variability (Figure 4b). In the NH, the positive polarity of the northern annular mode is linked to a reduction in SAT variance at middle to high latitudes, consistent with a decrease in atmospheric blocking during periods when the extratropical jet is anomalously strong. In the SH, the SAM has a generally similar signature in SAT variance (Figure 4b). Overall, the σ ratio is less than unity across most of the Antarctic continent during the positive polarity of the SAM, including much of the interior of both East and West Antarctica and the north-west Peninsula (Figure 4b). The most notable regions of significantly increased variance are found over the north-eastern Peninsula and over East Antarctica in a region that stretches south from Halley to Amundsen-Scott. Overall, the range of observed σ ratio is much greater for the SAM than it is for the BAM, extending from 0.75 at Bellingshausen to 1.09 at Esperanza.

Results stratified by season (Figure S7) indicate that the large decreases in SAT variance associated with the positive polarity of the SAM originate primarily from winter and spring, whereas the increases centred near Halley come from the autumn and summer seasons. These broad features are both reproducible in data for the first and second halves of the record (not shown). The sign of the station-based results is comparable to those derived from ERA-Interim at most locations during most seasons, but there are notable discrepancies as well. For example, in autumn the observations reveal a σ ratio significantly greater than unity at Esperanza, whereas ERA-Interim data have values significantly less than unity. This difference between results based on station data and ERA-Interim may be due to sampling variability but also likely reflects shortcomings in the ability of the reanalysis to properly simulate the role of the fine-scale regional orography in SAT variability [*van Lipzig et al.*, 2008], as suggested by the Δrmse SAT value between the two data sets being significantly larger for Esperanza than any other station (cf. Table 1).

Figures 4c and 4d show results based on year-round data for the PSA1 and PSA2 patterns, respectively. In general, the signatures of the PSA1 and PSA2 patterns in SAT variance are most significant (and reproducible) over the western hemisphere (Figure 4c), despite the observation that both patterns have widespread signatures in Antarctic mean SAT across both the western and eastern hemispheres (Figures 3c and 3d). Over the western hemisphere, the most pronounced changes in daily SAT variance over Antarctica are coincident with similarly signed changes in mean SAT (Figure 3c) and eddy activity (Figure 2c). For example, the positive PSA1 pattern is associated with increased SAT variance across the Ross Ice Shelf and much of inland West Antarctica (Figure 4c), where both eddy activity (Figure 2c) and SATs (Figure 3c) are anomalously positive. Conversely, it is associated with decreased SAT variance near the Filchner-Ronne Ice Shelf and western East Antarctica including Amundsen-Scott station, where both eddy activity (Figure 2c) and SATs (Figure 3c) are anomalously negative. These primary centres of action are present in both the ERA-Interim reanalysis and station-based observations. Over the continent, the PSA2 pattern is associated with generally similar relationships between eddy activity, mean SAT, and SAT variance. We note that, as defined here, the positive phase of the PSA1 and PSA2 patterns generally have an opposite effect on Antarctic SAT variance across the western hemisphere (cf. Figures 4c and 4d). The most robust signatures in SAT variance over
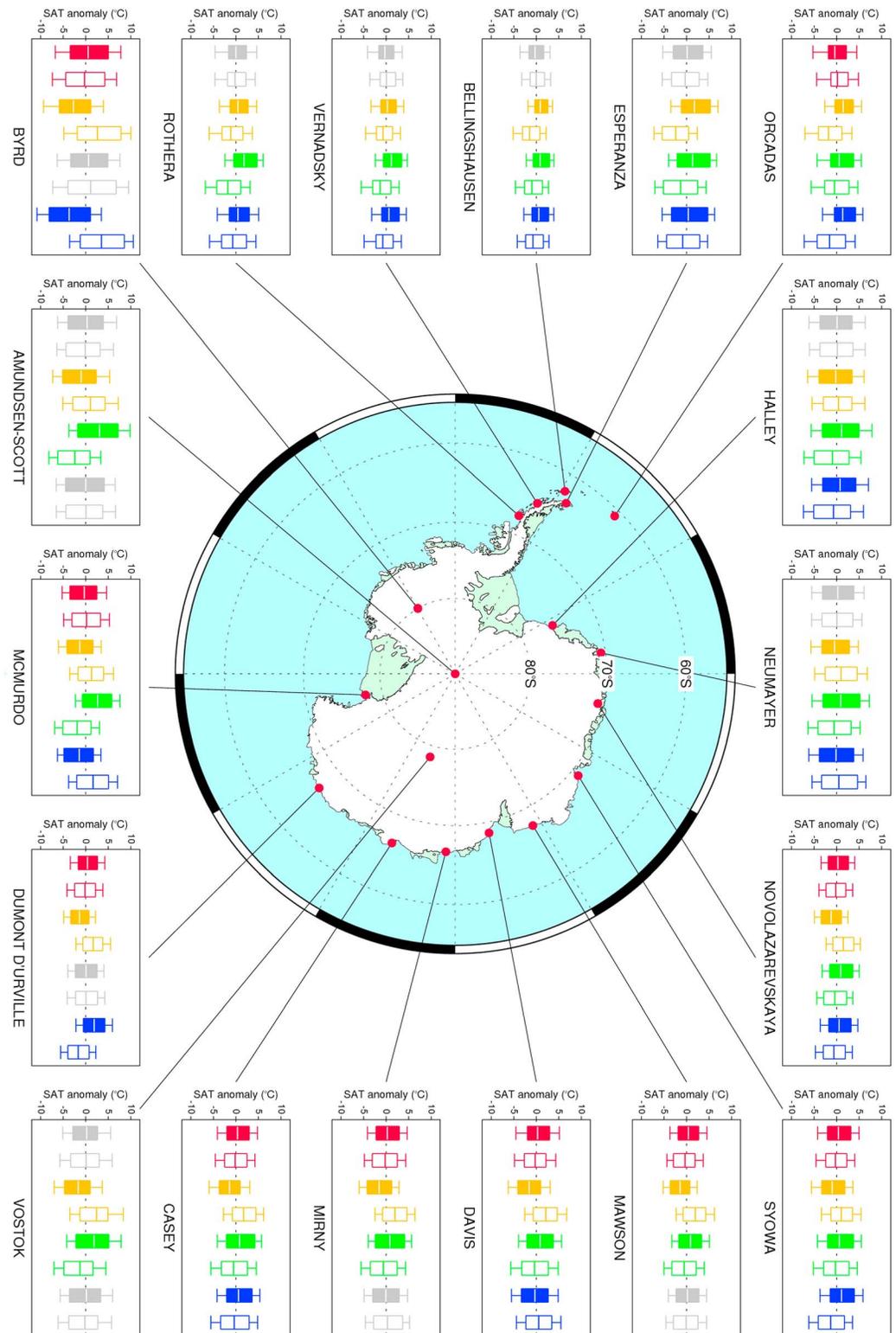
Figure 5. The distribution of SAT anomalies associated with the positive (colored box) and negative (transparent box) phases of the circulation patterns at the 18 meteorological stations. Cases where the differences in mean SAT anomalies are not significantly different at the $p < 0.05$ level are shown in gray; cases where the differences are significant are shown in color: red for the BAM, yellow for the SAM, green for the PSA1 pattern, and blue for the PSA2 pattern. The boxes represent the range of values between the upper and lower quartiles, with the mean shown as a horizontal line, and the whiskers represent one standard deviation away from the mean.

the western part of the continent are reproducible from one season to the next (Figures S8 and S9). However, the seasonally varying signatures of the PSA1 and PSA2 patterns in SAT variance over other regions of Antarctica, particularly over the eastern hemisphere, are noisy and thus difficult to interpret.

5. Discussion and Conclusions

Antarctic SAT plays a critical role not only in Antarctic climate but also global climate. Over Antarctica, it is directly linked to regional melting and indirectly linked to the availability of moisture and thus snowfall [*Krinner et al.*, 2007; *Ligtenberg et al.*, 2013]. Globally, Antarctic SAT has the potential to affect sea level through its influence on surface melting and the stability of ice shelves that fringe the continent and buttress the ice behind [*Scambos et al.*, 2004].

Arguably, understanding and predicting future changes in Antarctic SATs requires an understanding of the processes that govern their variability on shorter timescales. This point is emphasized by the observation that significant SAT trends of opposing sign in different regions of Antarctica have occurred in the past few decades [e.g., *Nicolas and Bromwich*, 2014]. These have been partially ascribed to anthropogenically forced changes in circulation [e.g., *Thompson and Solomon*, 2002; *Marshall et al.*, 2006] and changes in the strength and nature of tropical teleconnections to Antarctica [e.g., *Ding et al.*, 2011; *Schneider et al.*, 2012].

The purpose of this study is to build on our understanding of Antarctic SAT variability by assessing their spatially and seasonally varying relationships with the four principal patterns of SH extratropical circulation variability—the BAM, SAM, and two PSA patterns. To do so, we have exploited daily mean data from both ERA-Interim (which provides continent-wide sampling but is also in part model derived) and 18 Antarctic stations (which provide raw observations). Our use of daily data affords both a relatively large sample size (i.e., SAT varies on submonthly timescales) and also the ability to assess the signatures of large-scale climate variability in the day-to-day variance of Antarctic SATs.

Figure 5 provides a summary of the signatures of all four circulation patterns in the station-based SAT anomalies. As discussed in the main text, and indicated in both Figures 3 and 5, the BAM has a significant effect on mean temperature over parts of East Antarctica (primarily in winter) but otherwise has by far the weakest signature on Antarctic SATs of all four circulation patterns. In contrast, the SAM has a statistically significant impact on mean SAT at all the Antarctic stations examined here (Figures 3 and 5), and the reanalysis data indicate that this holds true for almost all of the continent (Figure 3). The spatial relationship between the SAM and daily mean SAT anomalies is broadly temporally invariant across the four seasons (Figure S3). The signatures of the PSA patterns are most pronounced over the western hemisphere (Figures 3 and 5) but—as is especially the case for the PSA1 pattern—also extend to eastern Antarctica. Both PSA patterns have a significantly weaker amplitude on Antarctic SATs during summer, reflecting the magnitude of the seasonality of the SH response to ENSO [e.g., *Jin and Kirtman*, 2009].

The *variance* in SAT also plays an important role in determining regional climate, but for the most part, the impacts of the circulation patterns on the variance of Antarctic SAT are weaker than they are for mean SAT (cf. Figures 4 and 5). Again, the BAM has the weakest signature of the four patterns. The SAM has a much more robust signature, with the positive polarity of the SAM generally linked to reduced SAT variability across most of the continent (Figure 4). One of the few regions that has increased variance associated with the positive polarity of the SAM is the eastern side of the Peninsula. This may result from the impact of relatively local-scale warm föhn winds in this region, which are more frequent under conditions of stronger zonal flow [e.g., *Marshall et al.*, 2006]. The influence of the two PSA patterns on the variance of Antarctic SAT is mostly limited to the western hemisphere, and the positive phase of the two patterns generally has an opposite effect on the variance of SAT (cf. Figures 4c and 4d). The range in the σ ratio at the stations varies from 0.75 (SAM: Bellingshausen) to 1.18 (PSA1: Amundsen-Scott).

The results shown here are consistent with but also build upon those indicated in previous studies. The signature of the SAM in Antarctic SAT has been explored in numerous previous works [e.g., *Kwok and Comiso*, 2002; *Thompson and Solomon*, 2002; *Marshall*, 2007], but those studies generally rely on year-round data and/or monthly mean data and have not explored the signature of the SAM in the variance of SAT. Preceding studies have examined the linkages between ENSO Antarctic SATs in the context of the PSA1 pattern [*Schneider et al.*, 2012] and the seasonal warming in West Antarctica [*Ding et al.*, 2011]. But the results

shown here are the first to (1) reveal that the impact of the PSA1 pattern on SAT encompasses almost all of Antarctica, (2) explore the linkages between the PSA2 across the whole continent in all seasons, and (3) examine the impact of the BAM on Antarctic SAT.

The findings in this study have been derived from daily data. But to the extent that the relationships between the circulation and surface temperature are not strongly dependent on timescale, they also provide insights into variability in Antarctic SATs on longer timescales. The projected changes in the SAM in response to increasing greenhouse gases and ozone recovery are broadly consistent among current climate models [e.g., *Arblaster et al.*, 2011; *McLandress et al.*, 2011]. The projected future changes in ENSO and its PSA teleconnection patterns are less clear [e.g., *Stevenson et al.*, 2012]. Based on the results of this study, an issue of particular relevance to Antarctic SATs is the ability of models to simulate the SH response to SST variability in the eastern and central Pacific, which have been linked to the PSA1 and PSA2 patterns, respectively [e.g., *Rodrigues et al.*, 2015]. We have not assessed in detail the temporal stationarity of the relationships described in this study. Some studies imply that the relationship between the SAM and SATs indicated in Figure 3b has changed in some regions of Antarctica during periods of the observational record [*Silvestri and Vera*, 2009; *Marshall et al.*, 2013]. Nevertheless, our analyses of subsets of the data suggest that the broad-scale climate linkages identified here are robust enough to use as benchmarks for both (1) assessing the ability of numerical models to simulate the linkages between dynamic variability and Antarctic SATs and (2) interpreting the Antarctic climate response to future changes in tropical sea surface temperatures, ozone recovery, and greenhouse gas increases.

References

Arblaster, J. M., G. A. Meehl, and D. J. Karoly (2011), Future climate change in the Southern Hemisphere: Competing effects of ozone and greenhouse gases, *Geophys. Res. Lett.*, 38, L02701, doi:10.1029/2010GL045384.

Bracegirdle, T. J., and G. J. Marshall (2012), The reliability of Antarctic tropospheric pressure and temperature in the latest global reanalyses, *J. Clim.*, 25, 7138–7146, doi:10.1175/JCLI-D-11-00685.1.

Bromwich, D. H., J. P. Nicolas, A. J. Monaghan, M. A. Lazzara, L. M. Keller, G. A. Weidner, and A. B. Wilson (2013), Central West Antarctica among the most rapidly warming regions on Earth, *Nat. Geosci.*, 6, 139–145, doi:10.1038/NGEO1671.

Cape, M. R., M. Vernet, P. Skvarca, S. Marinsek, T. Scambos, and E. Domack (2015), Foehn winds link climate-driven warming to ice shelf evolution in Antarctica, *J. Geophys. Res. Atmos.*, 120, 11,037–11,057, doi:10.1002/2015JD023465.

Dee, D. P., et al. (2011), The ERA-Interim reanalysis: Configuration and performance of the data assimilation system, *Q. J. R. Meteorol. Soc.*, 137, 553–597, doi:10.1002/qj.828.

Ding, Q., E. J. Steig, D. S. Battisti, and M. Küttel (2011), Winter warming in West Antarctica caused by central tropical Pacific warming, *Nat. Geosci.*, 4, 398–403, doi:10.1038/NGEO1129.

Fogt, R. L., D. H. Bromwich, and K. M. Hines (2011), Understanding the SAM influence on the South Pacific ENSO teleconnection, *Clim. Dyn.*, 36, 1555–1576, doi:10.1007/s00382-010-0905-0.

Fogt, R. L., J. M. Jones, and J. Renwick (2012a), Seasonal zonal asymmetries in the Southern Annular Mode and their impact on regional temperature anomalies, *J. Clim.*, 25, 6253–6270, doi:10.1175/JCLI-D-11-00474.1.

Fogt, R. L., A. J. Wovrosh, A. Langen, and I. Simmonds (2012b), The characteristic variability and connection to the underlying synoptic activity of the Amundsen-Bellingshausen Seas low, *J. Geophys. Res.*, 117, D07111, doi:10.1029/2011JD017337.

Gong, D., and S. Wang (1999), Definition of Antarctic Oscillation Index, *Geophys. Res. Lett.*, 26, 459–462, doi:10.1029/1999GL900003.

Hartmann, D. L., and F. Lo (1998), Wave-driven zonal flow vacillation in the Southern Hemisphere, *J. Atmos. Sci.*, 55, 1303–1315.

Hosking, J. S., A. Orr, G. J. Marshall, J. Turner, and T. Phillips (2013), The influence of the Amundsen-Bellingshausen Sea low on the climate of West Antarctica and its representation in coupled climate model simulations, *J. Clim.*, 26, 6633–6648, doi:10.1175/JCLI-D-12-00813.1.

Jin, D., and B. P. Kirtman (2009), Why the Southern Hemisphere ENSO responses lead ENSO, *J. Geophys. Res.*, 114, D23101, doi:10.1029/2009JD012657.

Jones, P. D., and D. H. Lister (2015), Antarctic near-surface air temperatures compared with ERA-Interim values since 1979, *Int. J. Climatol.*, 35, 1354–1366, doi:10.1002/joc.4061.

Kidson, J. W. (1988), Interannual variations in the Southern Hemisphere circulation, *J. Clim.*, 1, 1177–1198.

Krinner, G., O. Magand, I. Simmonds, C. Genthon, and J.-L. Dufresne (2007), Simulated Antarctic precipitation and surface mass balance at the end of the twentieth and twenty-first centuries, *Clim. Dyn.*, 28, 215–230, doi:10.1007/s00382-006-0177-x.

Kwok, R., and J. C. Comiso (2002), Spatial patterns of variability in Antarctic surface temperature: Connections to the Southern Hemisphere Annular Mode and the Southern Oscillation, *Geophys. Res. Lett.*, 29(14), 1705, doi:10.1029/2002GL015415.

Lee, T., W. R. Hobbs, J. K. Willis, D. Halkides, I. Fukumori, E. M. Armstrong, A. K. Hayashi, W. T. Liu, W. Patzert, and O. Wang (2010), Record warming in the South Pacific and western Antarctica associated with the strong central-Pacific El Niño in 2009–10, *Geophys. Res. Lett.*, 37, L19704, doi:10.1029/2010GL044865.

L'Heureux, M. L., and D. W. J. Thompson (2006), Observed relationships between the El Niño-Southern Oscillation and the extratropical zonal-mean circulation, *J. Clim.*, 19, 276–287.

Ligtenberg, S. R. M., W. J. van de Berg, M. R. van den Broeke, J. G. L. Rae, and E. van Meijgaard (2013), Future surface mass balance of the Antarctic ice sheet and its influence on sea level change, simulated by a regional atmospheric climate model, *Clim. Dyn.*, 41, 867–884, doi:10.1007/s00382-013-1749-1.

Marshall, G. J. (2003), Trends in the Southern Annular Mode from observations and reanalyses, *J. Clim.*, 16, 4134–4143.

Marshall, G. J. (2007), Half-century seasonal relationships between the Southern Annular Mode and Antarctic temperatures, *Int. J. Climatol.*, 27, 373–383, doi:10.1002/joc.1407.

Marshall, G. J., A. Orr, N. P. M. van Lipzig, and J. C. King (2006), The impact of a changing Southern Annular Mode on Antarctic Peninsula summer temperatures, *J. Clim.*, 19, 5388–5404.

Marshall, G. J., A. Orr, and J. Turner (2013), A predominant reversal in the relationship between the SAM and East Antarctic temperatures during the twenty-first century, *J. Clim.*, *26*, 5196–5204, doi:10.1175/JCLI-D-12-00671.1.

McLandress, C., T. G. Shepherd, J. F. Scinocca, D. A. Plummer, M. Sigmond, A. I. Jonsson, and M. C. Reader (2011), Separating the dynamical effects of climate change and ozone depletion. Part II: Southern Hemisphere troposphere, *J. Clim.*, *24*, 1850–1868, doi:10.1175/2010JCLI3958.1.

Mo, K. C. (2000), Relationships between low-frequency variability in the Southern Hemisphere and sea surface temperature anomalies, *J. Clim.*, *13*, 3599–3610.

Mo, K. C., and R. W. Higgins (1998), The Pacific-South American modes and tropical convection during the Southern Hemisphere winter, *Mon. Weather Rev.*, *126*, 1581–1596.

Mo, K. C., and J. N. Paegle (2001), The Pacific-South American modes and their downstream effects, *Int. J. Climatol.*, *21*, 1211–1229, doi:10.1002/joc.685.

Nicolas, J. P., and D. H. Bromwich (2014), New reconstruction of Antarctic near-surface temperatures: Multidecadal trends and reliability of global reanalyses, *J. Clim.*, *27*, 8070–8093, doi:10.1175/JCLI-D-13-00733.1.

North, G. R., T. L. Bell, R. F. Cahalan, and F. J. Moeng (1982), Sampling errors in estimation of empirical orthogonal functions, *Mon. Weather Rev.*, *110*, 699–706.

Polvani, L. M., M. Previdi, and C. Deser (2011), Large cancellation, due to ozone recovery, of future Southern Hemisphere atmospheric circulation trends, *Geophys. Res. Lett.*, *38*, L04707, doi:10.1029/2011GL046712.

Previdi, M., and L. M. Polvani (2014), Climate system response to stratospheric ozone depletion and recovery, *Q. J. R. Meteorol. Soc.*, *140*, 2401–2419, doi:10.1002/qj.2330.

Previdi, M., K. L. Smith, and L. M. Polvani (2013), The Antarctic atmospheric energy budget. Part I: Climatology and intraseasonal-to-interannual variability, *J. Clim.*, *26*, 6406–6418, doi:10.1175/JCLI-D-12-00640.1.

Raphael, M. N. (2004), A zonal wave 3 index for the Southern Hemisphere, *Geophys. Res. Lett.*, *31*, L23212, doi:10.1029/2004GL020365.

Raphael, M. N., G. J. Marshall, J. Turner, R. L. Fogt, D. P. Schneider, D. A. Dixon, J. S. Hosking, J. M. Jones, and W. H. Hobbs (2016), The Amundsen Sea Low: Variability, change and impact on Antarctic climate, *Bull. Am. Meteorol. Soc.*, *97*, 111–121, doi:10.1175/BAMS-D-14-00018.1.

Robertson, A. W., and C. R. Mechoso (2003), Circulation regimes and low-frequency oscillations in the South Pacific sector, *Mon. Weather Rev.*, *131*, 1566–1576.

Rodrigues, R. R., E. J. D. Campos, and R. Haarsma (2015), The impact of ENSO on the South Atlantic subtropical dipole mode, *J. Clim.*, *28*, 2691–2705, doi:10.1175/JCLI-D-14-00483.1.

Scambos, T. A., J. A. Bohlander, C. A. Shuman, and P. Skvarca (2004), Glacier acceleration and thinning after ice shelf collapse in the Larsen B embayment, Antarctica, *Geophys. Res. Lett.*, *31*, L18402, doi:10.1029/2004GL020670.

Schneider, D. P., Y. Okumura, and C. Deser (2012), Observed Antarctic interannual climate variability and tropical linkages, *J. Clim.*, *25*, 4048–4066, doi:10.1175/JCLI-D-11-00273.1.

Sigmond, M., M. C. Reader, J. C. Fyfe, and N. P. Gillett (2011), Drivers of past and future Southern Ocean change: Stratospheric ozone versus greenhouse gas impacts, *Geophys. Res. Lett.*, *38*, L12601, doi:10.1029/2011GL047120.

Silvestri, G., and C. Vera (2009), Nonstationary impacts of the Southern Annular Mode on Southern Hemisphere climate, *J. Clim.*, *22*, 6142–6148, doi:10.1175/2009JCLI3036.1.

Stevenson, S., B. Fox-Kemper, M. Jochum, R. Neale, C. Deser, and G. Meehl (2012), Will there be a significant change to El Niño in the twenty-first century? *J. Clim.*, *25*, 2129–2145, doi:10.1175/JCLI-D-11-00252.1.

Thompson, D. W. J., and E. A. Barnes (2014), Periodic variability in the large-scale Southern Hemisphere atmospheric circulation, *Science*, *343*, 642–645, doi:10.1126/science.1247660.

Thompson, D. W. J., and J. M. Wallace (2000), Annular modes in the extratropical circulation. Part I: Month-to-month variability, *J. Clim.*, *13*, 1000–1016.

Thompson, D. W. J., and J. D. Woodworth (2014), Barotropic and baroclinic annular variability in the Southern Hemisphere, *J. Atmos. Sci.*, *71*, 1480–1493, doi:10.1175/JAS-D-13-0185.1.

Thompson, S. W. J., and S. Solomon (2002), Interpretation of recent Southern Hemisphere climate change, *Science*, *296*, 895–899, doi:10.1126/science.1069270.

Turner, J. (2004), The El-Niño-Southern Oscillation and Antarctica, *Int. J. Climatol.*, *24*, 1–31.

Turner, J., S. R. Colwell, G. J. Marshall, T. A. Lachlan-Cope, A. M. Carleton, P. D. Jones, V. Lagun, P. A. Reid, and S. Iagovkina (2004), The SCAR READER project: Toward a high-quality database of mean Antarctic meteorological observations, *J. Clim.*, *17*, 2890–2898.

van den Broeke, M. R., and N. P. M. van Lipzig (2003), Response of wintertime Antarctic temperatures to the Antarctic Oscillation: Results of a regional climate model, in *Antarctic Peninsula Climate Variability: Historical and Paleoenvironmental Perspectives*, edited by E. Domack, et al., pp. 43–58, AGU, Washington, D. C., doi:10.1029/AR079p0043.

Van Lipzig, N. P. M., G. J. Marshall, A. Orr, and J. C. King (2008), The relationship between the Southern Hemisphere annular mode and Antarctic Peninsula summer temperatures: Analysis of a high-resolution model climatology, *J. Clim.*, *21*, 1649–1668, doi:10.1175/2007JCLI1695.1.

Wilks, D. S. (2006), *Statistical Methods in the Atmospheric Sciences*, 2nd ed., Elsevier, Amsterdam.

Wilson, A. B., D. H. Bromwich, K. M. Hines, and S.-H. Wang (2014), El Niño flavors and their simulated impacts on atmospheric circulation in the high southern latitudes, *J. Clim.*, *27*, 8934–8955, doi:10.1175/JCLI-D-14-00296.1.